JACS
JOURNAL OF THE AMERICAN CHEMICAL SOCIETY
Article
pubs.acs.org/JACS

Mechanisms of Halogen-Based Covalent Self-Assembly on Metal Surfaces

Jonas Björk,*[,†] Felix Hanke,[‡,¶] and Sven Stafström[†]

[†]Department of Physics, Chemistry and Biology, IFM, Linköping University, Linköping 581 83, Sweden
[‡]Surface Science Research Centre, Department of Chemistry, University of Liverpool, Liverpool L69 7ZD, U.K.

Supporting Information

ABSTRACT: We computationally study the reaction mechanisms of halogen-based covalent self-assembly, a major route for synthesizing molecular nanostructures and nanographenes on surfaces. Focusing on biphenyl as a small model system, we describe the dehalogenation, recombination, and diffusion processes. The kinetics of the different processes are also investigated, in particular how diffusion and coupling barriers affect recombination rates. Trends across the periodic table are derived from three commonly used close-packed (111) surfaces (Cu, Ag, and Au) and two halogens (Br and I). We show that the halogen atoms can poison the surface, thus hindering long-range ordering of the self-assembled structures. Finally, we present core-level shifts of the relevant carbon and halogen atoms, to provide reference data for reliably detecting self-assembly without the need for atomic-resolution scanning tunneling microscopy.

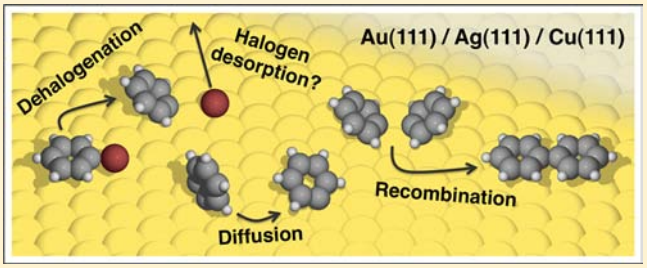

INTRODUCTION

Covalent self-assembly of molecular precursors on metallic surfaces is now a well-established route for growing an extensive range of atomically well-defined nanostructures,[1−11] and the graphene roadmap lists it as a promising avenue toward obtaining high-quality nanographenes.[12] This approach is extremely versatile, and the design of the product can, in principle, be controlled by the molecular precursors, the temperature, and the underlying surface. At this point, there are several challenges, including scaling-up production of high-quality nanostructures, characterizing the results in bulk and outside of the scanning tunneling microscope, and discovering new molecular precursors, which often involves significant amounts of trial and error. Here, we use extensive density functional electronic structure calculations to help resolve some of these challenges. In particular, we give a detailed description of the dehalogenation, recombination, and diffusion processes, providing reaction energies, barriers, and the core-level shifts associated with the reacting species.

The principle of halogen-based covalent self-assembly on surfaces was first demonstrated on Au(111) by Grill and co-workers,[1] who used the tetraphenylporphyrin molecule with specific hydrogen atoms replaced by bromine. Since bromine atoms split off at lower temperatures than their hydrogen counterparts, unsaturated carbon atoms at predefined positions are generated, enabling coupling into covalent dimers, 1D chains, and smaller 2D structures. Following these findings, several studies have illustrated the concept using molecular building blocks with specific hydrogens replaced by either bromine[2,3] or iodine,[5,6] or a combination of the two.[7] The theoretical reports about this type of self-assembly to date are limited to only a handful of studies,[6,13−15] and systematic studies, comparing trends of reactions over different surfaces by their reaction pathways, are still missing.

Halogen-based covalent self-assembly is associated with two fundamental reaction steps: (a) dehalogenation of the molecular precursors and (b) coupling reaction between the dehalogenated precursors. The second step is naturally dependent on the diffusion of the molecules on the surface. There are also several associated reactions taking place, such as diffusion and desorption of halogens. The latter is crucial for avoiding contamination of the substrate, since a high halogen concentration on the surface may hinder diffusion of molecules or promote recombination of halogens and dehalogenated precursors. All these processes depend critically on the underlying substrate, which acts as a catalyst for the dehalogenation and significantly influences the remaining chemical reactions.

The *a priori* prediction of the coupled product for a specific set of precursors on a particular surface presents a significant challenge. First of all, a systematic study of all possible pathways is required. Another crucial issue is that the characterization of these systems is dependent on scanning tunneling microscopy (STM), which has obvious limits to industrial up-scaling. There are only a few exceptions,[16] and reliable reference data for averaging techniques are needed to develop these approaches. In this paper, we tackle both of these issues using density functional theory (DFT)-based transition-state calculations. We consider both the dissociation of bromine and iodine from

Received: January 10, 2013
Published: March 18, 2013

dx.doi.org/10.1021/ja400304b | J. Am. Chem. Soc. 2013, 135, 5768−5775

aromatic hydrocarbons, and the concomitant coupling between dehalogenated products, on the commonly used close-packed (111) facets of Au, Ag, and Cu. As model reactions the formation of biphenyl from both bromobenzene (C_6H_5Br) and iodobenzene (C_6H_5I) is studied. In all relevant reaction steps we provide simulated core-level shifts (CLSs)—of C atoms and halogens—for reference in X-ray photoelectron spectroscopy (XPS) experiments. In Scheme 1 the two fundamental reaction steps are illustrated, namely the dehalogenation of bromobenzene (or iodobenzene) and the coupling of two phenyls into biphenyl.

Scheme 1. Reaction Diagrams of (a) Dehalogenation of a Halogen-Substituted Benzene Molecule into Phenyl (in This Study X = Br or I) and (b) Recombination of Two Phenyls into Biphenyl

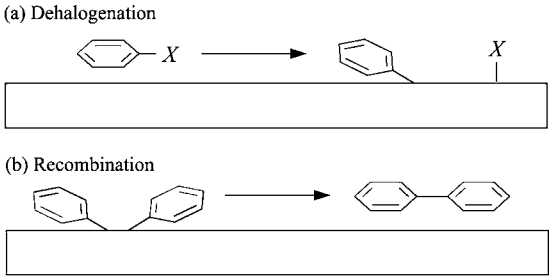

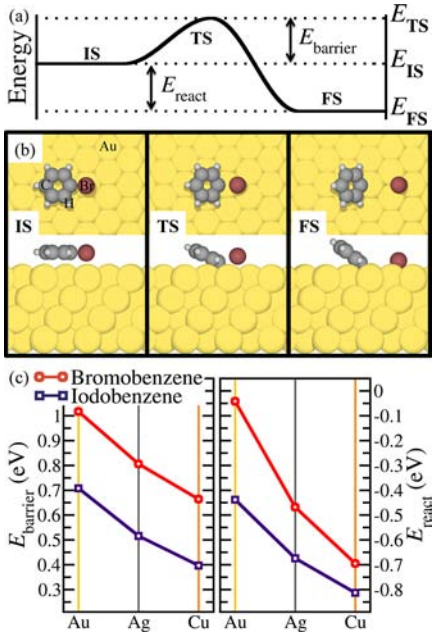

Figure 1. (a) Definitions of the energy barrier ($E_{barrier}$) and reaction energy (E_{react}) for dehalogenation reactions. (b) The dissociation of bromobenzene on Au(111), depicting top and side views of the initial state (**IS**), transition state (**TS**), and final state (**FS**) of the reaction. (c) $E_{barrier}$ (left) and E_{react} (right) for the dissociation of bromobenzene and iodobenzene on the (111) facets of Au, Ag, and Cu.

RESULTS AND DISCUSSION

Splitting-Off Bromine and Iodine from Molecular Precursors. The common initial step in halogen-based covalent self-assembly is the dissociation of halogens from the molecular precursors. Considering the dehalogenation of bromobenzene and iodobenzene in the gas phase, these reactions are highly endothermic, with reaction energies of 3.85 and 3.33 eV for bromobenzene and iodobenzene, respectively. This is due to the very unfavourable radical products. Our gas phase reaction energies were obtained by calculating energy differneces between the bromine (iodine) and phenyl separated in the gas phase and bromobenzene (iodobenzene) in the gas phase. For halogens and phenyl, spin-polarized calculations were performed.

To study how the (111) facets of the three metals affect the two dehalogenation reactions, transition-state calculations were carried out using the *nudged elastic band* (NEB)[17] and *Dimer*[18] methods. Figure 1 shows the initial, transition, and final states (denoted as **IS**, **TS**, and **FS**, respectively) of the bromobenzene dissociation on Au(111) and summarizes the calculated energy barriers ($E_{barrier} = E_{TS} - E_{IS}$) and reaction energies ($E_{react} = E_{FS} - E_{IS}$). The reaction mechanisms are very similar for both bromobenzene and iodobenzene on all three surfaces, as exemplified for bromobenzene on Au(111) in Figure 1b. The bromobenzene/iodobenzene molecule is physisorbed in the **IS**, while both the phenyl ring and the halogen are chemisorbed in the **FS**: the phenyl adsorbs with its unsaturated C-atom to a single substrate atom, while the halogen is adsorbed in a hollow site. The **TS** is associated with the halogen sitting near the hollow site closest to the bare C-atom for all paths, with a C–Br distance of 2.39 Å for Au, 2.43 Å for Ag, and 2.20 Å for Cu. This illustrates the importance of the lattice constants: the C–Br spacing in the **TS** is always about 80–85% of the nearest-neighbor spacing of the substrate surface. For the dissociation of iodine, the equivalent C–I distances follow a similar trend, although the C–I distances are about 0.1–0.2 Å larger than the C–Br lengths (see Supporting Information (SI) for details about relevant bond distances).

Figure 1c illustrates the trends of $E_{barrier}$ and E_{react} across the three surfaces. Both reactions are exothermic on all surfaces, reflected by the negative E_{react}. This is due to the final products being chemisorbed in the **FS**. In fact, the chemisorbed phenyl was found to be more stable than the physisorbed phenyl by at least 1.1 eV on all surface (see SI).

The dehalogenation is most favorable on Cu(111) and least favorable on Au(111), suggesting that Cu is the most reactive surface for dehalogenation while Au is the least reactive one. Furthermore, for a given surface the reaction is more exothermic for the dissociation of iodobenzene than for the dissociation of bromobenzene, consistent with the reaction energies in the gas phase (see above). However, moving from the surface that is least reactive for the dehalogenation (Au) to the most reactive one (Cu), the difference of E_{react} between splitting off bromine and iodine is reduced from 0.28 to 0.13 eV, while in the gas phase, the corresponding difference is 0.52 eV. On the surfaces the two reactions become closer in hierarchy, and the more reactive the surface, the smaller the difference of E_{react} between debromination and deiodonization.

The rate at which a reaction will proceed depends on $E_{barrier}$ rather than E_{react}. The values of $E_{barrier}$ are in the range 0.66–1.02 eV for the dissociation of bromobenzene, and 0.40–0.71 eV for the dissociation of iodobenzene, with the largest barrier for Au(111) and the smallest one for Cu(111) for each of the reactions. From comparison with the reaction energies in the gas phase it becomes clear that the metal surfaces have a strong catalytic effect on the dehalogenation. They significantly lower the energy barriers and thus decrease the temperature at which

dx.doi.org/10.1021/ja400304b | J. Am. Chem. Soc. 2013, 135, 5768–5775

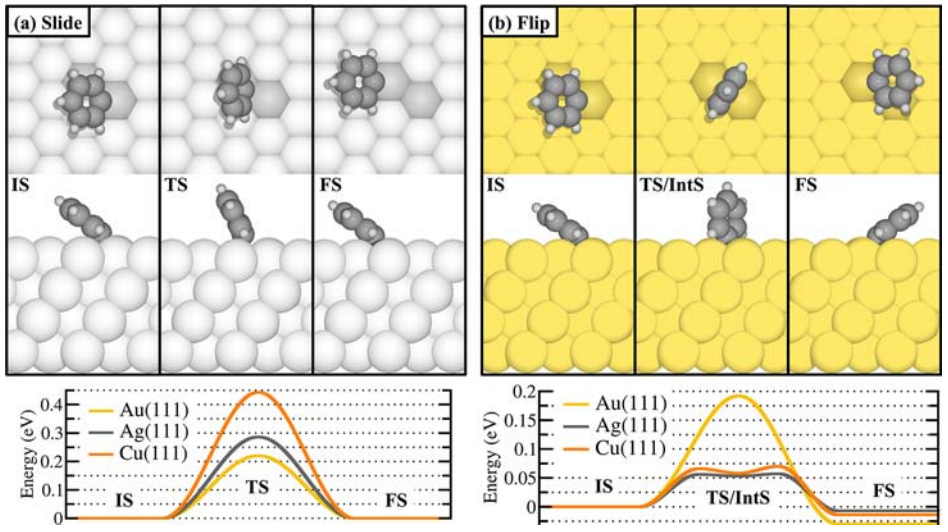

Figure 2. Energy diagrams for (a) sliding diffusion and (b) flipping diffusion of phenyl on Au(111), Ag(111), and Au(111), where the top and side views of the paths are depicted in the top panel for (a) Ag(111) and (b) Au(111). In both processes, phenyl diffuses between two surface atoms that are depicted darker than other surface atoms. Note that, on Au(111), the flipping and sliding diffusions have identical **TS**s and differ only by the relative orientation of the molecule in the **IS** and **FS**. The flipping diffusion (b) is a two-step process on Cu(111) and Ag(111). The small energy difference between **IS** and **FS** is induced by the orientation of phenyl with respect to the second (and third) surface layer.

the reactions take place effectively, while leaving the substrate in its original condition.

As for E_{react}, $E_{barrier}$ follows the trend of the relative reactivity of the surfaces,[19] and the energy barrier for splitting off iodine is smaller than for bromine. Interestingly, the difference of $E_{barrier}$ between bromine and iodine is around 0.3 eV for all surfaces. Using molecular precursors containing both bromine and iodine, it has been illustrated that iodine splits off at lower temperatures than bromine on Au(111). This is trivially due to the fact that the barrier for deiodonization is smaller than for debromination on Au(111). Our data strongly support this concept since the difference of $E_{barrier}$ between debromination and deiodonization is more or less constant for the surfaces. Therefore, we predict that similar hierarchical principles can be employed also on Ag(111) and Cu(111), in different temperature regimes.

Finally, we consider the correlation between $E_{barrier}$ and E_{react}. Interestingly, the two quantities are linearly dependent, following a Brønsted−Evans−Polanyi-type relationship, for the dissociation of both bromine and iodine; i.e., $E_{barrier}$ of these dehalogenation reactions can, in principle, be extrapolated for other surfaces if E_{react} is known (Figure S11).

Summarizing the dehalogenation results, the (111) facets of Au, Ag, and Cu significantly reduce the energy barrier associated with the dissociation of bromobenzene and iodobenzene. The surfaces not only act as a support, constraining the molecular motion into 2D, but also reduce the temperature required for the reactions to effectively occur. The two dehalogenation reactions are most energetically favorable and have the smallest reaction barriers for Cu(111), while they are least favorable and have the largest barriers for Au(111). For all surfaces the barrier of dissociation is smaller for iodine than for bromine. Thus, hierarchic two-step dehalogenation reactions, using precursors with both bromine and iodine that were recently reported on Au(111),[7] are also expected to work on Ag(111) and Cu(111), but in different temperature regimes.

Recombination of Dehalogenated Precursors. The dehalogenation barrier determines how easily the halogens split off from the molecular precursors. However, the final formation of the covalent nanostructures is governed by the reaction between surface-assisted radicals. The formation of biphenyl from two phenyl radicals occurs in two successive steps, precursor diffusion and coupling.

Phenyl can diffuse by either *sliding* or *flipping* between two adsorption sites. In the sliding diffusion, illustrated in Figure 2a, phenyl has the same orientation in the **IS** and **FS**. On all surfaces the sliding diffusion is associated with a single barrier, which is smallest for Au(111) and largest for Cu(111), and there is no clear correlation with the dehalogenation activity of the surfaces. In the **TS**, phenyl is much closer to an upright position compared to the **IS** and **FS**, with an inclination from the surface normal of 34° and 26° on Cu(111) and Ag(111), respectively, while it is adsorbed completely upright (no inclination) in the **TS** on Au(111).

Figure 2b illustrates the alternative type of diffusion, where phenyl flips from one site to another. This type of diffusion is a two-barrier process for Ag(111) and Cu(111), where an upright adsorption configuration constitues a shallow intermediate state. On Au, the flipping has only one barrier, where the upright configuration represents the **TS**, which is identical to the **TS** of the sliding diffusion. The barrier of the flipping diffusion is largest on Au(111), while it is considerably smaller for Ag(111) and Cu(111). These barriers were defined as the difference between the highest- and lowest-energy configurations along the path.

For simple phenyl rings, the flipping diffusion is associated with considerably smaller energy barriers compared to the sliding diffusion, in agreement with a recent study for Cu(111).[14] However, the flipping barriers may not be transferable for the diffusion of larger molecules, which have a stronger physisorption and might favor a diffusion path with the molecular plane oriented more parallel to the surface. It has, for example, been shown that the diffusion of cyclohexa-*m*-phenylene, where a flat diffusion is acquired, has a significantly larger barrier on Cu(111) compared to Ag(111).[6] Furthermore, the diffusion of porphyrins on Cu(111) is driven by a combination of slide and rotation motion.[20] In summary,

dx.doi.org/10.1021/ja400304b | J. Am. Chem. Soc. 2013, 135, 5768−5775

flipping diffusion is unlikely for anything larger than a phenyl ring. This suggests that a critical difference between the various precursor molecules could be found in their diffusion behavior on different surfaces.

A high mobility of molecules is a prerequisite for the self-assembly of well-ordered networks.[6] In this respect, from the hierarchy of the (sliding) diffusion barriers, Cu(111) is the worst candidate. The measured barriers for the sliding and rotation barriers for tetraphenylporphyrin on Cu(111) are 0.71 ± 0.08 and 1.28 ± 0.12 eV, respectively,[20] comparable to our calculated dehalogenation barriers. Owing to the large molecular size, these numbers are significantly larger than our computed results for phenyl, suggesting that our results for diffusion should be taken as the lower limit. Furthermore, the presence of Cu adatoms may impact the self-assembly more than the poor diffusion on the atomically flat Cu(111) surface. These adatoms are known to have a great influence on self-assembly on Cu(111), where in many cases coordination bonds are formed instead of covalent networks.[21] The Cu adatoms can also contribute to the covalent bonding of the nanostructure.[22,23] Notably, sliding diffusion on Au(111) and Ag(111) has very similar barriers. A comparison of the diffusion behavior of other dehalogenated molecular building blocks would be of great interest for a more detailed analysis of these two surfaces.

Next we consider the coupling reaction of two phenyls. Inspired by a recent study on Cu(111),[14] an **IS** was used where the two phenyls are coordinated to the same surface atom. The coupling is depicted for Ag(111) in Figure 3, together with the energy diagram of the reaction on all three surfaces. Note that for the coupling the energy is not given with respect to the **IS**, but with respect to individual phenyls adsorbed on the respective surface. The **IS** contains information about the energy cost/gain for bringing two phenyls as close as possible to each other, without reacting. In fact, on all surfaces it costs energy to bring two phenyls together to the **IS**.

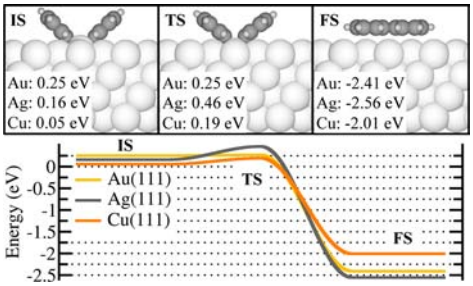

Figure 3. Energy diagram for the coupling reaction of two phenyls into biphenyl on the close-packed facets of Au, Ag, and Cu. In the top panel, the reaction is depicted for Ag(111), with the energy indicated for each of the states along the path for the respective surface. The energies are given with respect to the most stable adsorption configuration of an isolated phenyl on the respective surface.

The barrier separating the **FS** from **IS** is more or less nonexistent for Au(111): <0.01 eV, which is below the numerical resolution of our calculations. The coupling reaction has also a rather small barrier for Cu(111), while it is largest for Ag(111). Note that although no barrier separates the **FS** from the **IS** for Au(111), one needs to invest an energy of 0.25 eV to bring two well-separated phenyls to the **IS**. On all surfaces the recombination is highly exothermic. It has been illustrated that a large recombination barrier is beneficial for self-assembly of regular 2D networks,[6] in combination with a small diffusion barrier, as mentioned above. According to our results on the recombination and diffusion of phenyls, Ag(111) appears to be more suitable for covalent self-assembly than the most commonly used Au(111) surface. In fact, it has been illustrated that, in the self-assembly of cyclohexa-*m*-phenylene molecules, Ag(111) gives more regular 2D networks than both Au(111) and Cu(111).[6]

Putting together the results from dehalogenation, phenyl diffusion, and recombination of phenyls, dehalogenation clearly has the largest barrier. For halogen-based covalent self-assembly of small (benzene size) molecular precursors, the dehalogenation step is expected to be the rate-limiting one, as both diffusion and the coupling step are associated with small—and on Au(111) even negligible—barriers. However, with increasing the size of the molecular precursor, we expect that the self-assembly is limited by slow diffusion, as the molecules need to follow the sliding type of diffusion. Studies of the size dependence of the molecular precursors on the diffusion on the different surfaces would therefore be of great interest to control large-size self-assembled networks.

Impact of Halogen Byproducts. As mentioned above, both bromine and iodine are chemisorbed in the final state of the dehalogenation reactions and could interfere with the network formation. To generate largely self-assembled covalent domains, it is a prerequisite that the halogens can be removed from the surface. Otherwise the halogens will interfere with the self-assembly by hindering and/or recombining with dehalogenated molecules.

It was found that that the total energy cost of desorbing one halogen atomically is smaller compared to the total energy cost of desorbing two halogens as a molecule (Table S2). In fact, it was not possible to stabilize halogen molecules on either of the surfaces, since the halogen-surface interactions are much stronger than the halogen−halogen interactions. Thus, the halogens are much more likely to be desorbed atomically than molecularly, in agreement with literature.[5,24]

In Table 1, the binding energies of the two halogens on the three surfaces are summarized. The binding energies are around 3 eV for both halogens on all the surfaces. By comparing the dehalogenation barriers to the halogen binding energies, we can conclude that the desorption of the halogens from the surface is expected at considerably higher temperatures than their dissociation from the organic molecules.

Table 1. Binding Energies (in eV) of Atomic Bromine and Iodine on Cu(111), Ag(111), and Au(111), as Well as Calculated ($E_{coh.}^{calc}$) and Experimental[25] ($E_{coh.}^{exp}$) Cohesive Energies of These Metals

	bromine	iodine	$E_{coh.}^{calc}$	$E_{coh.}^{exp}$
Cu(111)	3.19	2.97	3.77	3.49
Ag(111)	3.23	3.01	2.92	2.95
Au(111)	2.80	2.76	3.54	3.81

One of the problems with the thermal desorption of halogens is the co-desorption of physisorbed nanostructures from the surface. However, the binding energy of physisorbed molecules is additive, and on Au(111) in the range 70−140 meV per carbon atom (depending on the hydrogen-to-carbon ratio).[15] Consequently, molecules with several tens of carbon atoms will stay physisorbed on the surface at temperatures where the halogens are efficiently desorbed.

dx.doi.org/10.1021/ja400304b | J. Am. Chem. Soc. 2013, 135, 5768−5775

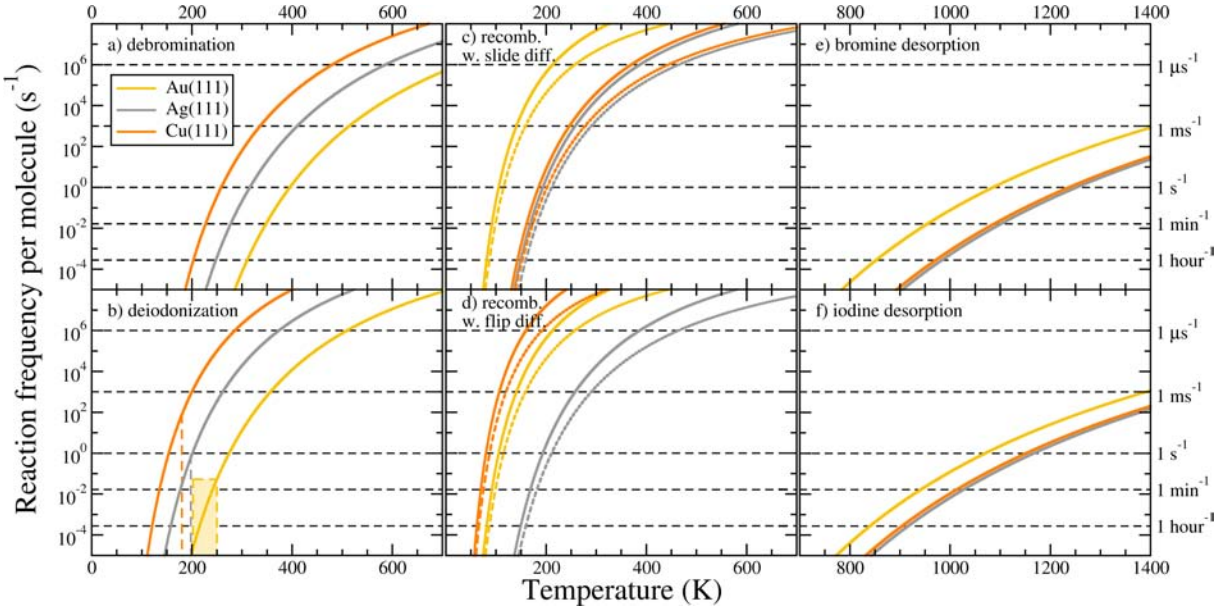

Figure 4. Reaction rates of the (a) debromination, (b) deiodonization, (c,d) biphenyl formation, and desorption of (e) bromine and (f) iodine for Cu(111), Ag(111), and Au(111). In (a,b,e,f) the rates were calculated by the Arrhenius equation $\nu = A\exp(-E_{barrier}/k_BT)$, using the computed energy barriers in Table S1, and a pre-exponential factor (A) of 10^{13} s^{-1}. For the recombination (c,d), rates are given for a coverage of 0.1 ML (solid lines) and 0.01 ML (dashed lines) of phenyl molecules. Furthermore, the recombination rates were calculated by considering both the (c) sliding and (d) flipping types of diffusion; see the Methods section for details. In (b) the experimentally determined deiodonization temperatures are indicated with dashed vertical lines for Cu[27,28] and Ag,[24] and as a temperature range for Au,[29] indicated by the shaded area.

Other problems that can arise when annealing to remove of chemisorbed halogen atoms are thermal reconstruction of the surface and thermally generated metal adatoms that interfere with the dehalogenated intermediates. The latter is a well-documented phenomenon for Cu(111), where the Cu adatoms incorporate into nanostructures already at low temperatures, resulting in, for example, metal−organic frameworks[21] or covalent structures where the adatoms take part in covalent bonding instead of forming carbon−carbon bonds.[22,23] Furthermore, halogens desorb as CuX from the Cu(111) surface, where X is the halogen.[26] This may appear as an unexpected result, as the cohesive energy of Cu is considerably larger than the binding energy of both bromine and iodine. However, the co-desorption of a Cu and halogen atom is associated with the availability of Cu adatoms rather than melting of the Cu crystal. Nevertheless, as already mentioned above, Cu(111) is not an ideal candidate for halogen-based covalent self-assembly.

Ag has a cohesive energy slightly smaller than the binding energies of both atomic iodine and bromine. However, it has been experimentally observed that iodine desorbs atomically from Ag(111) above 800 K.[5,24] Our results show that the desorption temperature of bromine is higher than that of iodine, and the question remains whether bromine also desorbs atomically from Ag(111). As shown in the previous section, this surface has great potential for forming ordered 2D networks in terms of diffusion and recombination of dehalogenated precursors. With iodine-substituted precursors, the halogen byproducts can be desorbed from the surface. This is also expected for the Au(111) surface, for which the binding energies of both bromine and iodine are smaller than the computed cohesive energy of the Au crystal by about 0.7 eV.

We also computed diffusion barriers of the halogens, and the results are summarized in Figure S18. In their diffusion, the halogens hop between inequivalent face-centered cubic hollow and hexagonally close-packed hollow sites, while the transition state is found to be on the bridge site. Despite the strong chemisorption of the halogens to the metals, the barriers are small, in the range 50−100 meV, suggesting that the halogens have a high mobility at experimental self-assembly temperatures. The barrier is largest on Au(111), while it is smallest on Cu(111), following a trend similar to the flipping diffusion of phenyls on the three surfaces.

Although the halogens can be desorbed atomically from Ag(111) and Au(111), this will only occur at significantly higher temperatures than the self-assembly of the covalent networks. During the self-assembly process the halogens are present on the surface, possibly hindering the formation of well-ordered networks. A plausible way of avoiding this problem could be to trap the halogens at specific areas on the surface. This might be done by designing chemically reactive areas to attract and subsequently trap the halogen atoms. The halogens are expected to find, and occupy, these areas faster than the dehalogenated molecules due to their small diffusion barriers and higher binding energies compared to the network precursors. An alternative approach would be to use substrates with a weaker adsorption of the halogens, in order to decrease the desorption temperatures of halogens. This could, for example, include metal alloys tailor-made for this purpose.

Reaction Rates. Based on the density functional results presented so far, we can provide insights into several issues relating to the kinetics of the self-assembly process, namely the overall rate-limiting step, the conditions under which halogens can be desorbed from the surface, and the lifetime of the intermediates on the surface. The last question is important for measuring the progress of the self-assembly reaction.

To investigate how the reaction kinetics is affected by the barriers of the different processes, reaction rates were calculated for the dehalogenation processes, the phenyl−phenyl recombination, and halogen desorption (Figure 4). Except for the

recombination, all rates were obtained from the Arrhenius equation $\nu = A\exp(-E_{barrier}/k_BT)$, with the commonly used prefactor $A = 10^{13}$ s^{-1}. The rate of recombination (ν_{recomb}) is much less trivial, as it necessarily has to involve both the rates of phenyl−phenyl coupling (ν_{couple}) and phenyl diffusion ($\nu_{diffuse}$) as derived in the Methods section. For ν_{recomb} we note two limits:

$$\nu_{recomb} = \theta\nu_{couple} \quad \text{if } \nu_{diffuse} \ll \nu_{couple} \tag{1}$$

and

$$\nu_{recomb} = \theta\nu_{diffuse} \quad \text{if } \nu_{diffuse} \gg \nu_{couple} \tag{2}$$

where θ is the coverage of molecules, with $\theta = 1$ corresponding to a fully covered surface.

The recombination frequency ν_{recomb} for Au(111) is independent of the type of diffusion, since both diffusions have the same barrier. For Ag(111), the flipping and sliding diffusions give almost identical E_{recomb}, despite the fact that $E_{diffuse}$ differs considerably between the two types of diffusion. This is due to the relatively large barrier of phenyl−phenyl coupling on this surface, resulting in E_{recomb} described by eq 1. For Cu(111), ν_{recomb} is highly dependent on the diffusion type, since for the sliding diffusion it is described by eq 2, while for the flipping diffusion it is described by eq 1.

The only case where the phenyl intermediates may be stabilized is for iodobenzene on Ag(111), where the recombination follows a similar trend as the deiodonization. For all other systems, the dehalogenation is expected at considerably higher temperatures than the recombination. This means that, subsequent to the dehalogenation, the phenyls will recombine immediately, with no possibility of detecting the phenyl intermediates on the surface. However, this is not necessarily true for larger molecules, where both diffusion and coupling have larger barriers than for phenyl, and dehalogenated intermediates have even been observed.[6]

The halogen desorption occurs at significantly higher temperatures than both recombination and dehalogenation, as discussed in the previous section. For the formation of biphenyl from bromobenzene and iodobenzene, our overall results give the following hierarchy of the temperatures of dehalogenation (T_{dehalo}), recombination (T_{recomb}), and halogen desorption ($T_{X\text{-}desorb}$):

$$T_{recomb} \lesssim T_{dehalo} \ll T_{X\text{-}desorb} \tag{3}$$

Comparing the combined rate of phenyl−phenyl coupling ν_{recomb} with the Arrhenius rate of dehalogenation in Figure 4 shows that the rate-limiting step in the simple model system considered here is indeed the dehalogenation. However, this might change for larger molecules with large diffusion barriers, which can become comparable to the dehalogenation barrier.[20] The full kinetic study of sufficiently large systems remains an outstanding challenge at present.

C(1s), Br(3d), and I(4d) Core-Level Shifts. Scanning tunneling microscopy is not convenient for all experimental situations. In particular, for a large-scale production of macromolecules and surface polymers, averaging techniques are more suitable as characterization tools. As such, XPS is a very powerful technique often employed in surface science, measuring the core-level binding energies. As these are highly dependent on the chemical environment of an atom, XPS gives direct insight into the chemical state of a system. In the case of chemical reactions on surfaces, the state of the system before the reaction is generally known, while information about the system subsequent to the reaction is acquired. The CLSs between products and reactants provide such information. Although vast information about CLSs can be found in the literature, it is not trivial what core levels to expect from a given reaction. Theoretical CLSs of model reactions, such as the ones demonstrated here, are of great interest for experimental characterization.[8,10,30] The simulated CLSs give an accurate description of the chemical shifts measured by XPS. This has, for example, been illustrated in the polymerization of tetaazaperopyrene molecules on Cu(111), where XPS experiments and CLS simulations agree within 20 meV.[10]

Here we give the simulated CLSs of carbon atoms and halogens for the relevant systems—bromobenzene, iodobenzene, phenyl, and halogen atom—adsorbed on the three surfaces. The results are summarized in Figure 5. We distinguish between two types of carbon atoms. First are CH (or methine) carbons, which are C-atoms bonded to a hydrogen atom. These C-atoms have the same nearest neighbors in all systems. The second type of carbon is the chemically active one, which is bonded to bromine (iodine) in

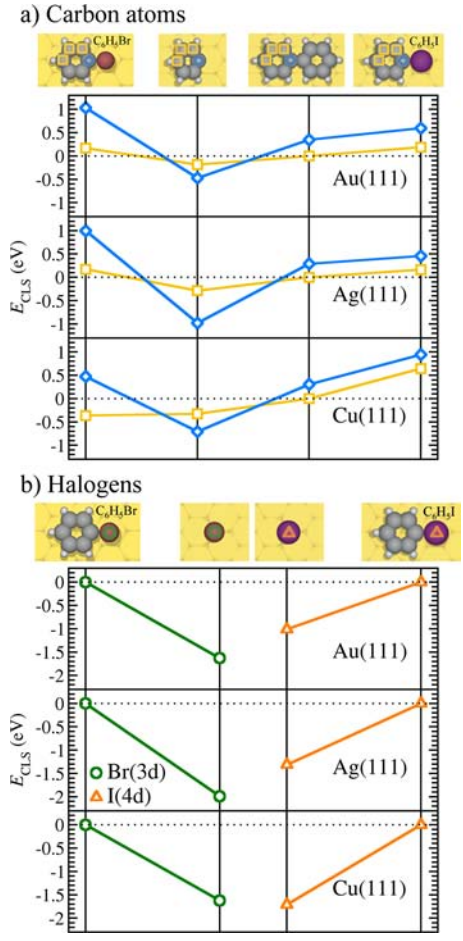

Figure 5. Simulated core-level shifts of (a) the C(1s), as well as (b) the Br(3d) and I(4d) core levels, for the systems depicted above each plot. For the methine C-atoms (C-atoms with an H-atom) the average CLSs are indicated. Furthermore, for C-atoms the CLSs are given with respect to the methine C-atoms in biphenyl adsorbed on the respective surface, while for bromine and iodine the CLSs are given with respect to the halogen in bromobenzene and iodobenzene, respectively. The expected error of the simulated CLSs is on the order of 10 meV.

dx.doi.org/10.1021/ja400304b | J. Am. Chem. Soc. 2013, 135, 5768−5775

bromobenzene (iodobenzene), is coordinated to a metal atom in phenyl, and has only carbon neighbors in biphenyl. The latter type of carbon is expected to experience the largest difference in core-level binding energy due to the variation of its chemical environment.

For the C(1s) core level, the C-atom with an adjoining Br-atom has a significantly larger core-level binding energy than other C-atoms. For iodobenzene, this difference is less pronounced. For phenyl, on the other hand, the C-atom bonded to the metal surface has a smaller core-level binding energy than the other C-atoms of the molecule. This provides a signature for noncoupled C-atoms, in particular on Ag(111). After formation of biphenyl, all C-atoms have similar core-level binding energies.

For the halogens, beginning with the 3d core level of bromine, the surface-bonded species is 1.6−1.9 eV lower in binding energy compared to bromine in bromobenzene. Subsequent to dehalogenation, a significant negative CLS is predicted for bromine. Also for the 4d core-level of iodine a negative, but smaller, CLS of 1.0−1.3 eV is expected as a result of the dehalogenation. In other words, the halogens provide the clearest signature when the dehalogenation of the C(1s) peak has occurred. In particular, the deconvolution of the C(1s) peak is often difficult in XPS data because in most cases the chemical environment is affected in only a small fraction of the C-atoms following a reaction, and is therefore difficult to resolve. [Note: For the Br(3d) and I(4d), XPS experiments always give a pair of peaks. This is due to the spin−orbit coupling of the core electrons in the final state, where the final state has either $J = 3/2$ or $J = 5/2$. The calculations presented here do not take into account the spin−orbit coupling in the final states but give the shift of the double-peak, where the internal energy difference between these two peaks is assumed to stay constant, independent of the chemical environment of the atom.]

The kinetics calculations indicated that the phenyl intermediates cannot be stabilized, since the recombination proceeds with a considerably higher rate than the dehalogenation (with one exception). Therefore, dehalogenated intermediates with small diffusion and coupling barriers are not predicted to be detectable in XPS experiments. However, these intermediates are expected to be detectable for very high diffusion or coupling barriers.

CONCLUSIONS

We have computationally studied the fundamental reactions in halogen-based covalent self-assembly on metal surfaces. To fully understand these reactions, we worked across the periodic table in two dimensions: metals and halogens. More specifically, we investigated the formation of biphenyl from bromobenzene and iodobenzene molecular precursors on the commonly employed (111) facets of three metals: Au, Ag, and Cu. The formation is associated with two fundamental reaction steps: dehalogenation and the concomitant coupling of dehalogenated molecular precursors. In addition to these elemental reactions, we have also studied the diffusion of phenyl and halogen atoms on the three surfaces, discussing the desorption of halogens from the surfaces, as well as simulated the core-level shifts for carbon and halogen atoms in all relevant reaction steps.

It was found that the metal surfaces effectively reduce the barriers to split off halogens, with the largest barrier for Au(111) and the smallest one for Cu(111). In other words, the surfaces are not only the inert supports where the dehalogenation can take plance, but also are instrumental in the dissociation. Furthermore, the barrier for dissociating iodine is smaller than that of bromine. It is predicted that the hierarchical principles using molecular precursors with both bromine and iodine can be utilized on Ag(111) and Cu(111), as it has been illustrated for Au(111).

Ag(111) and Au(111) have similar barriers for the sliding diffusion of phenyl. Furthermore, it was illustrated that Ag(111) has the largest barrier for recombination. In combination with the small diffusion barrier, this is desirable in covalent self-assembly. However, the halogen byproducts are expected to limit the formation of well-ordered structures. In particular, although the halogens can desorb atomically from Ag(111) and Au(111), this will occur at significantly higher temperatures than the self-assembly of the covalent networks.

We anticipate that a plausible solution to the problem of interfering halogens could be to trap these atoms at specific areas on the surface. This might be done by designing chemically reactive areas to attract and subsequently trap these atoms. An alternative approach would be to use substrates with a weaker adsorption of the halogens, in order to decrease the desorption temperatures of halogens. This could, for example, include metal alloys tailor-made for this purpose.

Finally, we simulated core-level shifts of carbon atoms and halogens in the various reaction steps. It was illustrated that dehalogenation gives a significant down-shift of the core level of the halogen in the range 1−2 eV, depending on the halogen and underlying surface. The CLSs of the halogens can be used to check whether the dehalogenation has proceeded or not, but they cannot confim network formation. Furthermore, the C(1s) core-level binding energy is significantly smaller for the carbon atoms that are coordinated to surface atoms. For relatively small molecular building blocks, these CLSs can be monitored experimentally by XPS, making it possible to follow exactly how far the reaction has proceeded without the need for scanning probe microscopy experiments.

METHODS

The calculations were carried out within the framework of periodic DFT using the VASP code.[31] The projected augmented wave method[32] was used to describe the ion−core electron interactions. van der Waals interactions were included using the van der Waals density functional (vdW-DF)[33] describing all nonlocal correlation energy, while local correlation energy was described by LDA. The exchange energy was described on the GGA level using the recently introduced optB86b functional.[34] This combination of exchange and correlation has shown to describe lattice constants very accurately,[34] while also providing a very good description of the vdW interactions between molecules and surfaces. Furthermore, a similar functional has shown to compare well with results obtained with the random phase approximation for a similar system.

All surfaces were modeled by four layered slabs separated by at least 15 Å of vacuum. For Au(111) and Ag(111) a $p(5\times5)$ surface unit cell was used, while for Cu(111) we used a $p(6\times6)$ surface unit cell. The larger unit cell of Cu(111) was used due the smaller lattice constant of Cu, to ensure well-separated molecules between repeated images. Calculated lattice constants of 4.140 Å for Au, 4.112 Å for Ag, and 3.598 Å for Cu were used (experimental lattice constants: 4.08, 4.09, and 3.61 Å for Au, Ag, and Cu, respectively[25]). Furthermore, all calculations were done with a 2×2 k-point sampling and a 500 eV kinetic energy cutoff. The relatively high cutoff ensures convergence of lattice constants when computed with the vdW-DF.

All structures were relaxed until the forces acting on the atoms in the molecules and the two uppermost layers of the slabs were smaller than 0.01 eV/Å.

Transition-state calculations were carried out with the VTST code,[35] using a combination of the *climbing image nudge elastic band*

dx.doi.org/10.1021/ja400304b | J. Am. Chem. Soc. 2013, 135, 5768−5775

(CI-NEB)[17] and *Dimer*[18] methods, as described in ref 15. For the CI-NEB calculations the number of images was adjusted specifically for each transition-state calculation such that the tangent along the path was well described. Typically 10−15 images were used in these calculations. The CI-NEB was used to find an initial estimate of the transition state. This estimate was then used to set up the starting configuration (central image and dimer) in the much quicker *Dimer* method. The structural optimization of the dimer was performed until the forces acting on the atoms on the central images were smaller than 0.02 eV/Å. The *Dimer* method allows the optimization of the transition state without taking into account the complete reaction path, thus reducing the computational cost compared to that of CI-NEB.

The reaction rate of the phenyl−phenyl recombination (ν_{recomb}) was estimated as a function of the surface coverage (θ), the phenyl diffusion rate (ν_{diffuse}), and the phenyl−phenyl coupling rate (ν_{couple}):

$$\nu_{\mathrm{recomb}} = \theta \frac{\nu_{\mathrm{couple}}\nu_{\mathrm{diffuse}}}{\nu_{\mathrm{couple}} + \nu_{\mathrm{diffuse}}} \quad (4)$$

In this model, we assume a single molecule diffusing in a randomly distributed field of other molecules. At any given time, the probability that the molecule has a nearest neighbor with which it can react is given by the coverage θ, and $\theta\nu_{\mathrm{diffuse}}$ is the rate at which the molecule meets a neighbor and has the possibility to react with another molecule. At this stage, the molecule can either couple with its neighbor or diffuse to the next site. The possibility for coupling is given by $\nu_{\mathrm{couple}}/(\nu_{\mathrm{couple}} + \nu_{\mathrm{diffuse}})$, resulting in eq 4. This model is valid for the small overall coverages typically encountered in the initial stages of a self-assembly process, as it is assumed that there are always empty neighboring sites to which phenyl can diffuse.

Simulated CLSs were obtained by comparing total energy differences between core-ionized and ground-state systems. The total energies of core-ionized systems were computed by using a core-ionized PAW potential for the core-ionized atom as described by Köhler and Kresse.[36] A separate calculation was carried out for every atom for which the CLS was computed. In previous studies, the CLSs obtained this way correlated with independent experimental results.[10]

■ ASSOCIATED CONTENT

Supporting Information

Computational details, additional figures, and data tables. This material is available free of charge via the Internet at http://pubs.acs.org.

■ AUTHOR INFORMATION

Corresponding Author

jonas.bjork@liu.se

Present Address

[¶]F.H.: Accelrys, 334 Science Park, Cambridge CB4 0WN, UK

Notes

The authors declare no competing financial interest.

■ ACKNOWLEDGMENTS

Funding was provided by the Swedish Research Council, and computer recourses were allocated by the National Supercomputer Centre, Sweden, through SNAC and the MATTER consortium.

■ REFERENCES

(1) Grill, L.; Dyer, M.; Lafferentz, L.; Persson, M.; Peters, M. V.; Hecht, S. *Nature Nanotechnol.* **2007**, *2*, 687−691.

(2) Cai, J.; Ruffieux, P.; Jaafar, R.; Bieri, M.; Braun, T.; Blankenburg, S.; Muoth, M.; Seitsonen, A. P.; Saleh, M.; Feng, X.; Müllen, K.; Fasel, R. *Nature* **2010**, *466*, 470−473.

(3) Huang, H.; Wei, D.; Sun, J.; Wong, S. L.; Feng, Y. P.; Neto, a. H. C.; Wee, A. T. S. *Sci. Rep.* **2012**, *2*, 983.

(4) Perepichka, D. F.; Rosei, F. *Science* **2009**, *323*, 216−217.

(5) Bieri, M.; Treier, M.; Cai, J.; Aït-Mansour, K.; Ruffieux, P.; Gröning, O.; Gröning, P.; Kastler, M.; Rieger, R.; Feng, X.; Müllen, K.; Fasel, R. *Chem. Commun.* **2009**, 6919−6921.

(6) Bieri, M.; Nguyen, M.-T.; Gröning, O.; Cai, J.; Treier, M.; Ait-Mansour, K.; Ruffieux, P.; Pignedoli, C. A.; Passerone, D.; Kastler, M.; Müllen, K.; Fasel, R. *J. Am. Chem. Soc.* **2010**, *132*, 16669−16676.

(7) Lafferentz, L.; Eberhardt, V.; Dri, C.; Africh, C.; Comelli, G.; Esch, F.; Hecht, S.; Grill, L. *Nature Chem.* **2012**, *4*, 215−220.

(8) Krasnikov, S. A.; Doyle, C. M.; Sergeeva, N. N.; Preobrajenski, A. B.; Vinogradov, N. A.; Sergeeva, Y. N.; Zakharov, A. A.; Senge, M. O.; Cafolla, A. A. *Nano Res.* **2011**, *4*, 376−384.

(9) Matena, M.; Riehm, T.; Stöhr, M.; Jung, T. A.; Gade, L. H. *Angew. Chem., Int. Ed.* **2008**, *47*, 2414−2417.

(10) Matena, M.; Stöhr, M.; Riehm, T.; Björk, J.; Martens, S.; Dyer, M. S.; Persson, M.; Lobo-Checa, J.; Müller, K.; Enache, M.; Wadepohl, H.; Zegenhagen, J.; Jung, T. A.; Gade, L. H. *Chem.—Eur. J.* **2010**, *16*, 2079−2091.

(11) Zhang, Y.-Q.; Kepčija, N.; Kleinschrodt, M.; Diller, K.; Fischer, S.; Papageorgiou, A. C.; Allegretti, F.; Björk, J.; Klyatskaya, S.; Klappenberger, F.; Ruben, M.; Barth, J. V. *Nat. Commun.* **2012**, *3*, 1286.

(12) Novoselov, K. S.; Fal'ko, V. I.; Colombo, L.; Gellert, P. R.; Schwab, M. G.; Kim, K. *Nature* **2012**, *490*, 192−200.

(13) Blankenburg, S.; Rauls, E.; Schmidt, W. G. *J. Phys. Chem. Lett.* **2010**, *1*, 3266−3270.

(14) Nguyen, M.-T.; Pignedoli, C. A.; Passerone, D. *Phys. Chem. Chem. Phys.* **2011**, *13*, 154−160.

(15) Björk, J.; Stafström, S.; Hanke, F. *J. Am. Chem. Soc.* **2011**, *133*, 14884−14887.

(16) Bronner, C.; Leyssner, F.; Stremlau, S.; Utecht, M.; Saalfrank, P.; Klamroth, T.; Tegeder, P. *Phys. Rev. B* **2012**, *86*, 085444−085448.

(17) (a) Henkelman, G.; Uberuaga, B. P.; Jónsson, H. *J. Chem. Phys.* **2000**, *113*, 9901−9904. (b) Henkelman, G.; Jónsson, H. *J. Chem. Phys.* **2000**, *113*, 9978−9985.

(18) (a) Henkelman, G.; Jónsson, H. *J. Chem. Phys.* **1999**, *111*, 7010−7022. (b) Kästner, J.; Sherwood, P. *J. Chem. Phys.* **2008**, *128*, 014106−014111.

(19) Hammer, B.; Norskov, J. K. *Nature* **1995**, *376*, 238−240.

(20) Buchner, F.; Xiao, J.; Zillner, E.; Chen, M.; Michael, R.; Ditze, S.; Stark, M.; Steinrück, H.-P.; Gottfried, J. M.; Marbach, H. *J. Phys. Chem. C* **2011**, 24172−24177.

(21) Björk, J.; Matena, M.; Dyer, M. S.; Enache, M.; Lobo-Checa, J.; Gade, L. H.; Jung, T. A.; Stöhr, M.; Persson, M. *Phys. Chem. Chem. Phys.* **2010**, *12*, 8815−8821.

(22) Haq, S.; Hanke, F.; Dyer, M. S.; Persson, M.; Iavicoli, P.; Amabilino, D. B.; Raval, R. *J. Am. Chem. Soc.* **2011**, *133*, 12031−12039.

(23) Hanke, F.; Haq, S.; Raval, R.; Persson, M. *ACS Nano* **2011**, *5*, 9093−9103.

(24) Szulczewski, G. J.; White, J. M. *Surf. Sci.* **1998**, *399*, 305−315.

(25) Kittel, C. *Introduction to Solid State Physics*, 8th ed.; John Wiley & Sons, Inc.: New York, 2005.

(26) Blake, M. M.; Nanayakkara, S. U.; Claridge, S. A.; Ferna, L. C.; Sykes, E. C. H.; Weiss, P. S. *J. Phys. Chem. A* **2009**, 13167−13172.

(27) Xi, M.; Bent, B. E. *Surf. Sci.* **1992**, *278*, 19−32.

(28) Xi, M.; Bent, B. E. *J. Am. Chem. Soc.* **1993**, *115*, 7426−7433.

(29) Syomin, D.; Koel, B. E. *Surf. Sci.* **2001**, *490*, 265−273.

(30) Doyle, C. M.; Krasnikov, S. A.; Sergeeva, N. N.; Preobrajenski, A. B.; Vinogradov, N. A.; Sergeeva, Y. N.; Senge, M. O.; Cafolla, A. A. *Chem. Commun.* **2011**, *47*, 12134−12136.

(31) Kresse, G.; Furthmüller, J. *Phys. Rev. B* **1996**, *54*, 11169−11186.

(32) (a) Blöchl, P. E. *Phys. Rev. B* **1994**, *50*, 17953−17979. (b) Kresse, G.; Joubert, D. *Phys. Rev. B* **1999**, *59*, 1758−1775.

(33) Dion, M.; Rydberg, H.; Schröder, E.; Langreth, D. C.; Lundqvist, B. I. *Phys. Rev. Lett.* **2004**, *92*, 246401−246404.

(34) Klimeš, J.; Bowler, D.; Michaelides, A. *Phys. Rev. B* **2011**, *83*, 195131−195143.

(35) The VTST code. http://theory.cm.utexas.edu/vtsttools/.

(36) Köhler, L.; Kresse, G. *Phys. Rev. B* **2004**, *70*, 165405−165413.